Infrared Quantum Dots**

By *Edward H. Sargent**

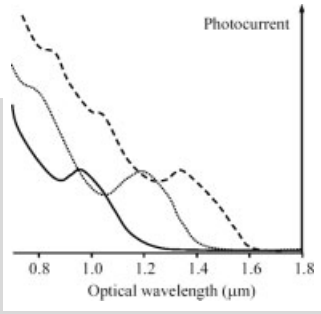

Colloidal nanocrystals are quantum-size-effect tunable; offer an abundance of available surface area for electronic and chemical interactions; and are processible from organic or aqueous solution onto substrates rigid or flexible, smooth or rough, flat or curved, inorganic or organic (including biological), crystalline or amorphous, conducting, semiconducting, or insulating. With the benefit of over a decade's progress in visible-light-emitting colloidal-quantum-dot synthesis, physical chemistry, and devices, significant progress has recently been made in infrared-active colloidal quantum dots and devices. This progress report summarizes the state-of-the-art in infrared colloidal quantum dots, with an emphasis on applications and devices. The applications of interest surveyed include monolithic integration of fiber-optic and free-space-communications photonic components with electronic substrates such as silicon and glass; in-vivo biological tagging in infrared spectral bands in which living tissue is optically penetrable to a depth of 5–10 cm; solar and thermal photovoltaics for energy conversion; and infrared sensing and imaging based on non-visible, including thermal, signatures. The synthesis and properties of quantum dots are first reviewed: photoluminescence quantum efficiencies greater than 50 % are achievable in solution, and stable luminescent dots are available in organic and aqueous solvents. Electroluminescent devices based on solution processing have been reported with external quantum efficiencies approaching 1 %. Photoconductive devices have been realized with 3 % internal quantum efficiencies, and a photovoltaic effect was recently observed. Electro-optic modulation achieved by either field- or charge-induced modification of the rate of optical absorption has been demonstrated based both on interband and intersubband (intraband) transitions. Optical gain from these processible materials with a threshold of 1 mJ cm^{-2} and an optical net modal gain coefficient of 260 ± 20 cm^{-1} have been reported.

1. The Need for Processible, Tunable Infrared-Active Optoelectronic Materials

While humans see only in the visible, our ability to communicate information, detect and treat disease, harness new forms of energy, and visualize threats to our safety and environment depend increasingly on mastery of the infrared spectral region.

Fiber-optic communications systems rely on the low-loss propagation of infrared optical signals inside pure glass fibers. An extended definition of the telecommunications wavelength band spans 1200–1700 nm.[1] It is of interest to unite, in a single monolithic fabrication process, the technologies which underlie optical communication, wireless, and wireline communications. Lattice-matched compound semiconductor epitaxy used in optoelectronics conflicts with convenient monolithic integration. In contrast, solution-processible active optoelectronic materials which provide a comprehensive set of canonical optoelectronic functions—light emission, detection, and modulation with customizable spectral response—facilitate the physical convergence of a diverse array of communications and computing technologies. Integration of active optoelectronics on a silicon chip is relevant to on-chip and chip-to-chip interconnection and line-of-sight free-space

[*] Prof. E. H. Sargent[+]
Nanotechnology and Photonics
MIT Microphotonics Laboratory
Massachusetts Institute of Technology
Cambridge, MA 02139-4307 (USA)
E-mail: tsargent@mit.edu

[+] Permanent address: Nortel Networks—Canada Research Chair in Emerging Technologies, Electrical & Computer Engineering, University of Toronto, Toronto, ON, M5S 1A1, Canada.

[**] The author acknowledges the contributions of Ahmed Maria, Ethan Klem, Fred Chang, Gerasimos Konstantatos, Ian Howard, Joe Salfi, Larissa Levina, Paul Cyr, Sam Cauchi, Scott Kuntze, Shiguo Zhang, Sjoerd Hoogland, Steve McDonald, and Vlad Sukhovatkin. Research presented herein was supported by Nortel Networks; the Ontario Centres of Excellence through Materials and Manufacturing Ontario, Photonics Research Ontario, Communications and Information Technology Ontario; the Ontario Research and Development Challenge Fund and the Ontario Innovation Trust; the Natural Sciences and Engineering Research Council of Canada through its Discovery Grant program, Collaborative Research and Development program, and Nano Innovation Platform; the Canada Foundation for Innovation; and the Canada Research Chairs Programme.

DOI: 10.1002/adma.200401552

communications, both for data communications and reliable friend/foe identification.[2]

Infrared optical imaging of living tissue is an area of growing interest. In the visible spectral region, functionally specific in-vivo cancer targeting and imaging have recently been demonstrated using semiconductor quantum dots. Systemic injection of multifunctional quantum-dot probes enabled sensitive and multicolored fluorescence imaging of cancer cells in vivo.[3] Using visible fluorescent tags, however, deep organs such as the liver and spleen could not be detected in mice because of the limited penetration depth of visible light. Deep-tissue imaging requires the use of infrared light within a spectral window separated from the major absorption peaks of hemoglobin and water. The use of near-infrared-emitting quantum dots is estimated to improve the tumor-imaging sensitivity at least tenfold, allowing sensitive detection of 10–100 cancer cells. High-transparency spectral bands centered at 840 nm, 1110 nm, 1320 nm, and 1680 nm[4] enable depths of detection of 5–10 cm,[5] a capability which recently provided surgeons with direct infrared visual guidance throughout a sentinel-lymph-node mapping procedure, minimizing incision and dissection inaccuracies and permitting real-time confirmation of complete resection.

Large-area, physically flexible photovoltaic sheets have recently received increasing attention as a low-cost, manufacturable, readily installed means of harnessing solar energy. While efforts have been primarily focused on the visible spectral region, infrared photovoltaics are also attracting attention. If the sun's spectrum is divided into its visible and infrared parts, the sun's intensity of approximately 970 $W\,m^{-2}$ includes approximately 490 $W\,m^{-2}$ of visible intensity (wavelengths < 0.7 μm) and 480 $W\,m^{-2}$ of infrared intensity. The visible portion of the spectrum could be used for direct lighting, and the infrared portion harnessed for electrical power, arguing for infrared photovoltaics.[6] Proponents of thermal photovoltaics propose generating electricity from combustion energy using photovoltaic cells that respond to infrared radiation from a fuel-fired emitter. Cogenerators of electricity and heat are proposed to be quiet, reliable, clean, and efficient, meeting the needs for remote and mobile applications.[7] A 1 cm^2 silicon cell in direct sunlight will generate about 0.01 W, but an efficient infrared photovoltaic cell of equal size could produce 1 W in a fuel-fired system.

Sensing and imaging already rely on the infrared spectral region. Were large-area, low-cost infrared sensitization of existing sensing and focal-plane-array technologies possible, the infrared could go from niche to ubiquity. The infrared spectral region manifests the thermal signatures of warm objects against a cold background and enables night vision based on infrared illumination. It can reveal spectral signatures of chemical species of interest in environmental monitoring and antiterrorism (biological and chemical threats): mid-infrared light (2.5–50 μm, 4000–200 cm^{-1}) excites characteristic molecular vibrations of particular utility that identify organic and organometallic molecules. Collision-avoidance sensors in the infrared exploit atmospheric-condition independence of select infrared wavelengths. Light curtains emit infrared light beams in front of a hazardous area being protected: a stop signal is sent to the guarded machine when any of the beams are blocked. Applications include perimeter guarding for industrial robots and machinery and point-of-access guarding for automated-machine assemblies.

This broad set of infrared-based applications point to the following set of requirements:

- A materials system that, rather than requiring lattice-matched epitaxial growth on perfect crystalline substrates, is compatible with solution processing and large-area devices, allowing the realization of devices on physically flexible substrates;
- A materials system that, through straightforward variation of synthetic parameters, allows controllable access to different portions of the broad infrared spectrum.

Prof. Sargent is the 2004–2005 Visiting Professor of Nanotechnology and Photonics in the Microphotonics Center at the Massachusetts Institute of Technology. He holds the Nortel Networks–Canada Research Chair in Emerging Technologies in the Edward S. Rogers Sr. Department of Electrical & Computer Engineering at the University of Toronto.

Prof. Edward (Ted) H. Sargent was in 2003 named one of the world's top young innovators by MIT's Technology Review magazine. He is author of well over one hundred papers published in international refereed journals and presented at international conferences. Since 2003 he has given invited lectures at Harvard, MIT, Caltech, Stanford, UCLA, UCSB, Oxford, Cambridge, and University College London. He has addressed scientific researchers at the leading technical conferences in the U.S., Japan, and Europe in the areas of nanotechnology, photonics, and optical networking. His research has been widely reported in the popular press including recent coverage in The Guardian, Wired, BusinessWeek, MSNBC, and National Geographic. In 2002, Prof. Sargent was celebrated by the Institute of Electrical and Electronics Engineers (IEEE), "For groundbreaking research in applying new phenomena and materials from nanotechnology towards transforming fibre-optic communications systems into agile optical networks." In 2004 he was named to Canada's Top 40 Under 40, a list of achievers across business, medicine, and science. Prof. Sargent received the B.Sc.Eng. (Engineering Physics) from Queen's University in 1995 and the Ph.D. in Electrical and Computer Engineering (Photonics) from the University of Toronto in 1998.

ADVANCED MATERIALS

Colloidal quantum dots satisfy these requirements: they may be processed from organic or aqueous solution using spin-casting, spray-coating, and blade- or drop-casting; their synthetic protocols may be extended to large-scale production; and their tailoring through the quantum-size effect has been widely explored.

Prior to the progress reported below, one key question remained: Could infrared devices be created which meet the demanding requirements of the above-mentioned applications—luminescence and photocurrent efficiencies and depths of modulation—within a colloidal-quantum-dot materials platform?

2. Colloidal Quantum Dots: Synthesis and Properties

We illustrate progress in infrared colloidal-quantum-dot synthesis by summarizing results for PbS, PbSe, and InAs.

PbS colloidal nanocrystals may be prepared using a solution-based organometallic route[8] using suitable precursors. PbO is dissolved in oleic acid and heated to 150 °C to produce a lead oleate precursor. The sulfur source bis(trimethylsilyl)-sulfide (TMS) in octadecene is added to the lead oleate solution, which is then removed from heat. The temperature is allowed to drop to below the nucleation-threshold temperature and maintained at the desired growth temperature. Oleic acid attaches to the surface of the nanocrystals, preventing them from aggregating and passivating the surface, thus reducing non-radiative recombination. The size of the nanocrystals is controlled by varying the concentration of the capping ligand; the injection temperature and injection time; the growth temperature and growth time; and the ratio of oleic acid to lead to sulfur. When the nanocrystals reach the desired size, they are precipitated by adding a polar solvent such as methanol and redispersed in a nonpolar solvent such as toluene. Figures 1a,b present transmission electron microscopy (TEM) images of dots synthesized by the organometallic route.

The size-dependent properties of quantum-confined states are illustrated in Figures 1c,d. The minimum transition energy in the limit of large dots is given by the bulk bandgap—0.41 eV in the case of PbS. The quantum-confined states within each band may be conceptualized in an envelope-function picture of a particle in a box of size and shape corresponding to the boundaries of the nanocrystals. Bulk PbS has reasonably symmetric bands: the effective mass of a hole is comparable to the effective mass of an electron, and the quantum-confined states are similarly spaced in the two bands. Formally, interband electronic transitions can only occur between electron and hole states with the same quantum numbers in the case of perfectly symmetric bands and confining-envelope potentials. For nanocrystals that are small relative to the Bohr radius of the bulk exciton, the quantization energies of electrons and holes are large compared to the Coulomb energy. In this regime, the Coulomb binding energy reduces the transition energy by a comparatively small amount. The Bohr exciton radius for PbS is 20 nm, for InAs, 34 nm, and for PbSe, 46 nm.[9] Syntheses of PbS, PbSe, and core–shell InAs/ZnSe typically result in dilute-solution photoluminescence quantum efficiencies in the range of 30–80 %.

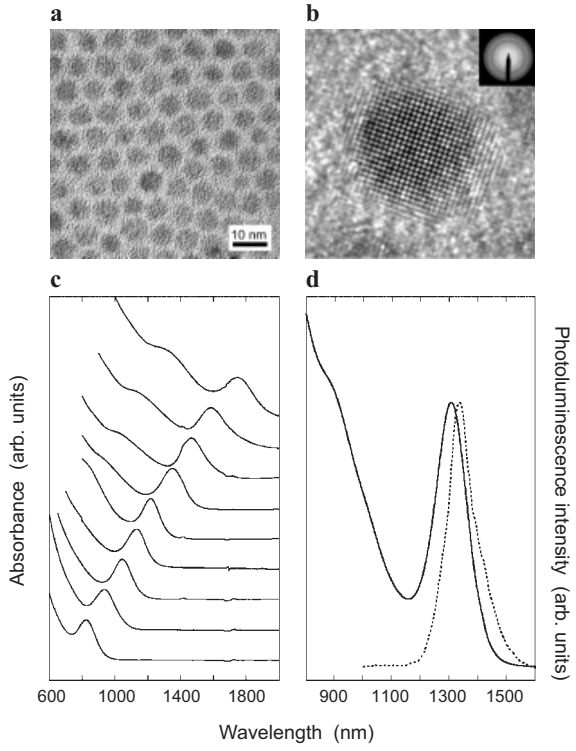

Figure 1. Physical properties of PbS quantum dots synthesized by an organometallic route. a,b) High-resolution TEM images of quantum dots with peak luminescence at 1440 nm. c) Absorption spectra of PbS dots with exciton peaks size-effect tuned from 800–1800 nm. d) Absorption and photoluminescence features of 6.5 nm diameter dots. Reprinted with permission from [8].

In contrast with the organometallic route, synthesis in aqueous solution is highly desirable for compatibility with biological assays. It also enables multilayer polymer/nanocrystal device fabrication for heterostructure engineering through the use of alternating aqueous/organic solvents in sequential layers. A one-stage water-based synthesis of stable and monodisperse PbS nanocrystals was recently reported to result in photo- and electroluminescence in the spectral range of 1000–1400 nm.[10] PbS nanocrystals were prepared in aqueous solutions using a mixture of thiols as a stabilizing agent. The combination of capping agents thioglycerol (TGL) and dithioglycerol (DTG) resulted in high-quality nanocrystals. $Pb(CH_3COO)_2$ and sodium sulfide were used as lead and sulfur sources. Size-effect tunability was demonstrated in the range of 1000–1400 nm. The combination of TGL and DTG in the appropriate ratio was necessary to obtain stable nanocrystals. The absolute photoluminescence quantum yield was determined to be 17 %.

The need for fluorophores stable in biological media is particularly urgent for in-vivo assays based on quantum dots emitting in the transparent tissue bands at 1050–1200 nm.

The growth of PbS nanoparticles on a DNA template has recently been demonstrated to result in efficient infrared fluorophores which are stable in blood plasma at 37 °C for over one week.[11] Quantum dots were grown on single-stranded DNA, as revealed in elementally resolved high-resolution TEM. The DNA phosphate backbone and imino protons provided sites for passivation and solubilization of the nanocrystals in aqueous solution. Photoluminescence quantum efficiencies as high as 11.5 % were obtained.

In the case of InAs, reports have included the synthesis of core–shell type I heterostructure dots with an InAs core, shape control over rods and tetrapods in InAs, detailed probing of intersubband transitions in InAs,[12,13] and evidence of long-sustained charging in InAs nanocrystals.[14]

Extensive time-resolved spectroscopy of visible and infrared nanocrystals has revealed some common trends, but also some quantitative variability. In the visible spectrum, holes are observed to relax more rapidly within the bands. In PbSe, nanocrystals capped with oleate ligands and having high quantum efficiencies revealed, at low pump powers, a first interband transition with a multi-exponential decay consisting of a 200 ps decay component and a very slow decay component which was attributed to slow radiative relaxation. Time-resolved photoluminescence studies have revealed a slow single-exponential decay with typical time constants in the vicinity of 1 μs. Carrier dynamics depend strongly on the nanocrystal surface, a fact which explains both variability amongst nominally similar experiments and differences in observed quantum efficiencies.

Auger recombination, a non-radiative process which depends on the preexistence of carriers in a band and thus grows strongly with both excitation and doping, has been studied extensively. Klimov et al. measured decay times of 10 ps for the 4-pair relaxation, 21 ps for the 3-pair relaxation, and 45 ps for the 2-pair relaxation.[15] In this vein, photoluminescence degradation has been observed in samples optically pumped over the course of hours. The effect has been ascribed to Auger ionization of the nanocrystal, giving rise to a long-lived charging and thus a dark state.[16] The nanocrystal remains in this dark state until the ejected carrier returns to the nanocrystal thermally or by tunneling, resulting in neutralization. It has similarly been proposed that photoionization results when a carrier is trapped on the surface of the nanocrystal and a further photon excites this carrier within its trap-state lifetime.

The influence of energy transfer among a population of closely spaced nanocrystals is one of importance in solid-state devices. It has been shown[17,18] that in pure nanocrystal films electron–hole pairs generated in smaller nanocrystals transfer to the larger ones. Photoluminescence measurements of mixed films have revealed quenching of the luminescence of the small dots and enhancement of the luminescence of the large dots.

3. Electroluminescent Devices

Electroluminescent sources in the infrared link electronics-based communications and signal-processing systems with the carriers used in optical communications. Measures of practical interest include external quantum efficiency—the ratio of photons extracted to electrons injected—and brightness. One inferred quantity often estimated and reported is the internal quantum efficiency—the number of photons generated per injected electron.

Infrared-light-emitting diodes based on colloidal nanocrystals have been fabricated[19] based on core–shell InAs/ZnSe quantum dots in a poly[2-methoxy-5-(2′-ethylhexoxy)-1,4-phenylenevinylene] (MEH–PPV) polymer blend, resulting in a reported external quantum efficiency of 0.5 % and an estimated internal quantum efficiency of 1 %. In these devices, the turn-on voltage exceeded 15 V. Size-tunable electroluminescence with internal efficiencies of 1.2 % was reported based on the core-only PbS system;[20] the efficiency has recently been improved to 3 %.[21] PbSe nanocrystal-monolayer devices[22] within a solution-processed and evaporated organic heterostructure were reported, with electroluminescence tunabilities of 1.3–1.55 μm demonstrated (Fig. 2a) and peak external efficiencies of 0.001 % obtained.

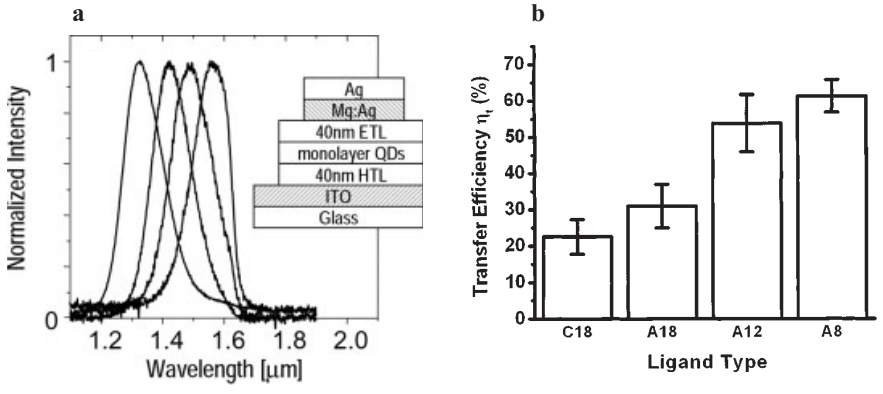

Figure 2. a) Electroluminescence spectra of a series of quantum-dot light-emitting devices tuned through the near infrared. Reprinted with permission from [21]. b) Absolute transfer efficiency of excitations from MEH–PPV to nanocrystals for four ligand choices: oleate (C18), octadecylamine (A18), dodecylamine (A12), and octylamine (A8). Reprinted with permission from [23]. Copyright 2004 American Institute of Physics.

ADVANCED MATERIALS

The exchange of surface-capping organic ligands on as-synthesized nanocrystals in favor of shorter insulating ligands appears to play a significant role in achieving high electroluminescence quantum efficiency devices. For example, precipitated PbS-nanocrystal powder was dissolved in a small amount of octylamine, the solution was heated at 50 °C for 24–48 h, and the resulting octylamine-capped nanocrystals were isolated by precipitation with a polar solvent.[20] The procedure was repeated to ensure uniform ligand exchange, and the final precipitate was dispersed into the desired organic solvent for polymer-composite fabrication. Whereas photoluminescence intensities for unexchanged and exchanged nanocrystal samples were comparable, the ~2 nm long oleate-capped nanocrystal devices exhibited a much lower electroluminescence intensity in the infrared than those capped with ~1 nm long octylamine ligands. It was noted that for electroluminescence, excitations generated within the polymer matrix must be transferred to the nanocrystals, and that the rate of energy transfer is presumably sensitive to both the choice of capping ligand and the proximity between exciton donor and acceptor.

This observation prompted subsequent investigations using photoluminescence excitation spectra of the influence of ligand chemistry and ligand length on energy transfer from a polymer matrix to nanocrystals.[23] PbS nanocrystals capped with as-synthesized oleate (~2 nm), octylamine (~1 nm), dodecylamine (~1.5 nm), and octadecylamine (~2 nm) ligands were combined with the host matrix MEH–PPV and formed into films. Composites based on as-synthesized PbS nanocrystals capped by oleate ligands provided transfer efficiencies—the number of excitons transferred to the nanocrystals divided by total number of excitons generated in the polymer—of 20 %. Replacing these ligands with the shortest ligands gave a threefold improvement in excitation-transfer efficiency (Fig. 2b).

The other pressing issue in achieving high electroluminescence quantum efficiency devices is the maximization of the internal efficiency of the nanocrystals in the solid state. A number of authors have remarked on an order-of-magnitude loss in photoluminescence quantum efficiency when processing PbS and PbSe quantum dots from solution into nanocrystal or nanocrystal/polymer composite films. Whereas thin-film photoluminescence quantum efficiencies in the vicinity of 1 % have typically been obtained, it has recently been shown that, by controlling the chemistry and packing fraction of quantum dots in polymers, photoluminescence quantum efficiencies as high as 12 % may be obtained in the solid state.[24]

The design of efficient electroluminescent devices has recently be considered from a theoretical standpoint.[25,26] These investigations have emphasized the importance of symmetry in the efficiency of electron and hole injection; of a sufficient areal cross-section of nanocrystals in the path of bipolar current; and of finding a concentration regime in which both energy-transfer efficiency and internal quantum efficiency can be maximized.

4. Photoconductive and Photovoltaic Devices

It is desired to harvest light efficiently in the infrared region in devices possessing characteristics such as ease of processing, low cost, physical flexibility, and large-area coverage. Sensitizing conjugated polymers with infrared-active nanocrystal quantum dots provides a spectrally tunable means of accessing the infrared while maintaining the advantageous properties of polymers.

A nanocomposite approach has recently been reported[27] in which quantum-size-effect-tuned PbS nanocrystals provide infrared sensitivity for MEH–PPV. This first report demonstrated the principle, but showed a very low efficiency of 10^{-5}, necessitating the use of modulated illumination and a lock-in amplifier to observe the photocurrent.

Recently demonstrated,[28] also using solution-processed materials, has been a three-orders-of-magnitude improvement in infrared photoconductive internal quantum efficiency compared to the previous result,[27] allowing observation of the photocurrent under continuous-wave illumination without reliance on lock-in techniques; an infrared photovoltaic effect was also observed for the first time in such materials. Under –5 V bias and illumination from a 975 nm laser, these detectors showed an internal quantum efficiency of 3 %, a ratio of photocurrent to dark current of 630, and a maximum responsivity of 3.1×10^{-3} AW^{-1} (Fig. 3a). The photovoltaic response under 975 nm excitation resulted in a maximum open-circuit voltage of ~0.36 V, a short-circuit current of 350 nA, and a short-circuit internal quantum efficiency of ~0.006 %. By varying the size of the nanocrystals during processing, photocurrent spectra were demonstrated with peaks tailored to 980 nm, 1.200 μm, and 1.355 μm (Fig. 3b).

This first report of a photovoltaic effect in PbS/MEH–PPV nanocomposites suggested that the system may form a type II heterostructure in which, following optical absorption resulting in the generation of an exciton, electrons remain confined to the nanocrystal while holes separate into the polymer. This suggests that the mechanism of excitation in forward-biased electroluminescence devices must indeed be energy-transfer based, given that separate electron and hole capture is not an energetically favored event. That both electroluminescent and photovoltaic devices may be realized in this one bulk structure suggests the need for nanocrystal/ligand/polymer heterojunction systems more specifically optimized to the application in question.

5. Optical Modulation: Interband and Intersubband

Electric-field-induced modulation of absorption in PbS nanocrystal quantum dots across the spectral region 600–2000 nm, which more than encompasses the entire telecommunications band, has recently been demonstrated. The device architecture consisted of PbS nanocrystals synthesized via the

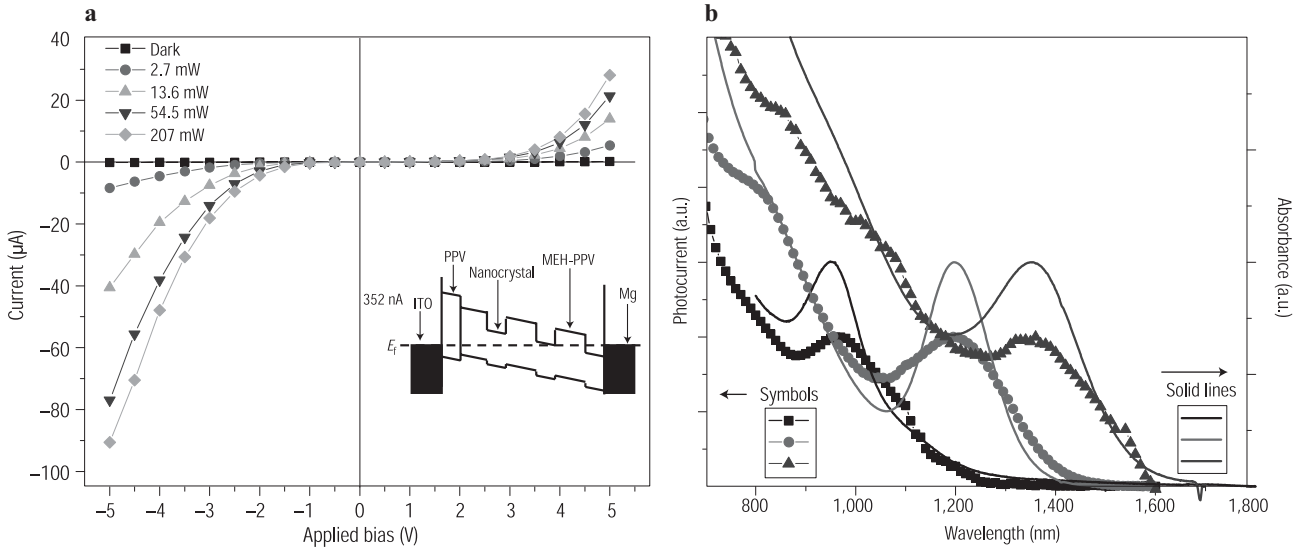

Figure 3. a) Photocurrent for a sample with ~90 wt.-% nanocrystals in the polymer/nanocrystal blend. The pump powers are shown in the legend. Inset: Proposed simplified band diagram after the Mg electrode has been deposited and the sample reaches equilibrium. b) Photocurrent spectral response (symbols) and the corresponding absorption spectra (solid lines) for three different samples. In each sample, the photocurrent response closely follows the absorption of the nanocrystals. The sample absorption peaks are tuned to 955 nm, 1200 nm, and 1355 nm. Reproduced from [28]. Copyright 2004 Nature Publishing Group.

organometallic route and sandwiched between SiO_x films. The bottom 360 nm thick dielectric layer was thermally evaporated onto a glass substrate overcoated with indium tin oxide (ITO), which served as the bottom electrical contact. Nanocrystal films ~700 nm thick were spin-coated onto the SiO_x-covered substrate and then overcoated with a top layer of 150 nm thick SiO, followed by a 5 nm layer of Au as a top electrical contact.

A sine-wave voltage was applied with amplitudes between 25 V and 65 V. Monochromatic light was incident perpendicular to the sample surface and thus parallel to the direction of the applied field. The electroabsorption signal reported was acquired at twice the frequency of the applied voltage via lock-in detection, and from the signal the change in absorption per unit length was determined. We show in Figure 4 for 5 nm and 7 nm diameter nanocrystals the unmodulated absorption (Figs. 4a,b) and the measured change in absorption due to the modulated applied electric field (Figs. 4c,d). The insets of Figures 4a,b show the set of optical transitions revealed in the quantum dots as a result of the sensitive electroabsorption spectroscopy provided by these measurements. These transitions correspond to the negative lobes of the electroabsorption spectrum. The dependence of the amplitude of the measured electroabsorption signal on applied peak voltage at each of the first three optical transitions revealed a

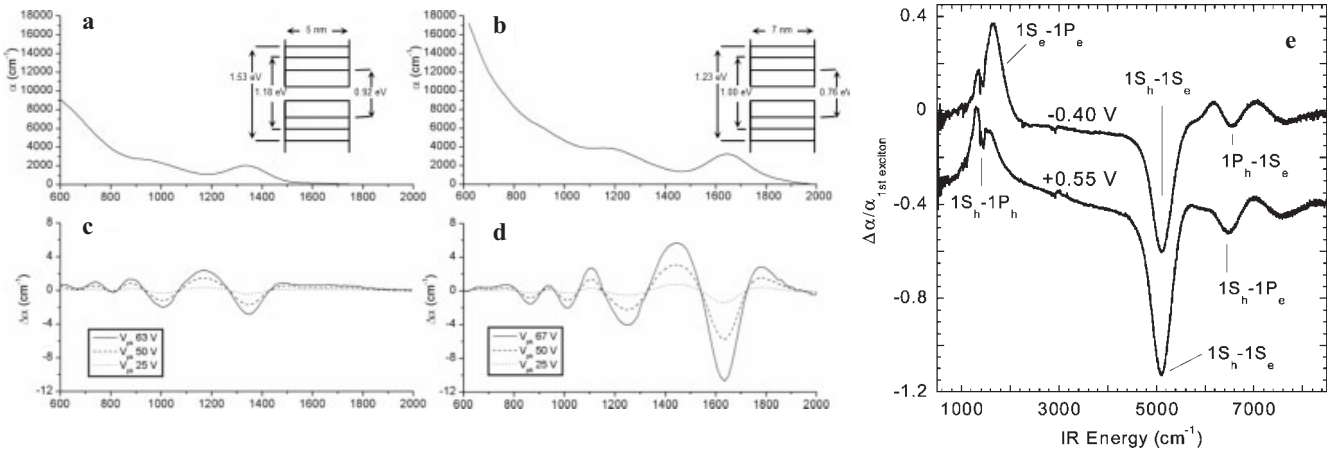

Figure 4. a,b) Unmodulated absorption spectra and c,d) electroabsorption spectra for devices based on 5 nm (a,c) and 7 nm (b,d) PbS nanocrystals. The insets show the transitions corresponding to the first three peaks in the measured electroabsorption spectrum. e) The change in absorption coefficient in PbSe quantum dots in an electrochemical cell under bias. Reproduced with permission from [29]. Copyright 2003 American Chemical Society.

ADVANCED MATERIALS

quadratic dependence on field. The maxima in the electroabsorption spectra closely correspond to the positions of the first excitonic peak, confirming the predominance of excitonic broadening as the basis for the observed effect.

Modulation based on charge injection, lowering the rate of interband transitions by occupying final states and enabling intersubband transitions by configuring carriers in the required initial states, has been demonstrated in a variety of electrochemical-cell configurations. Hole injection into quantum-confined states has been explored in PbSe,[29] with the corresponding spectroscopic changes measured (Fig. 4e). The exploitation of intersubband transitions, already widely exploited in epitaxial semiconductors, give promise for 2–10 μm modulators, detectors, and light emitters. While the electrochemical approach gives a very strong absorption change, its timescale of operation tends to be measured in seconds, whereas a number of applications would benefit from at least kilohertz response times.

6. Optical Gain

Room-temperature amplified spontaneous emission and spectral narrowing at infrared wavelengths have been reported in solution-processed films made up of both PbSe[30] and PbS[31] quantum-dot nanocrystals. The results are relevant to optical amplification and, ultimately, the possibility of realizing lasers integrated on a variety of substrates. In the case of PbSe, spectral narrowing and optical gain (Fig. 5a) were reported in an inorganic sol–gel titania matrix. In the case of PbS, the active optical medium provided amplified spontaneous emission at 1300 nm (Fig. 5c) and operated at room temperature without any additional matrix material, providing an optical gain of 260 cm^{-1} and a pump threshold of 1 mJ cm^{-2} (Fig. 5b). Nanocrystals synthesized in aqueous solution and stabilized using short ligands resulted in a high quantum-dot volume fraction in solid films and a three-dimensional superlattice effect which red-shifts emission relative to absorption.

7. Challenges and Future Prospects

The applications presented in the introduction to this Progress Report demand a variety of different performance specifications from processible infrared optoelectronic materials.

Optoelectronic integration for the unification of communications and computing platforms demands the merging of sources, detectors, and modulators onto a single chip. As shown herein, each of these device types has been demonstrated individually, but the set of processes and a prototype which unify them remain to be elaborated. Ultimately, the challenges associated specifically with integration on a silicon substrate—the canonical platform for electronics—need to be addressed. In all electrically injected polymer-based devices, the problem of charge-transport lengths and traversing inorganic/organic interfaces is of urgent importance. It would be of tremendous interest to exploit the outstanding electrical properties of crystalline silicon, and from it, to transfer energy,[32] without the requirement of separately transferring electrons and holes, across silicon/polymer/quantum dot interfaces. The use of silicon nanocrystals[33] may provide a first means of addressing the paucity of excitons in bulk silicon at room temperature.

Significant narrowing of the spectral shape of emission, detection, and modulation to the scale of one coarse wavelength-division multiplexed channel—20 nm—would further enhance the value of quantum-dot-based approaches. This hinges on creating dots with room-temperature homogeneous linewidths in the vicinity of 10 meV and on reducing inhomogeneous broadening to this order.

Electroluminescence efficiencies stand to be improved, principally through further enhancements to infrared quan-

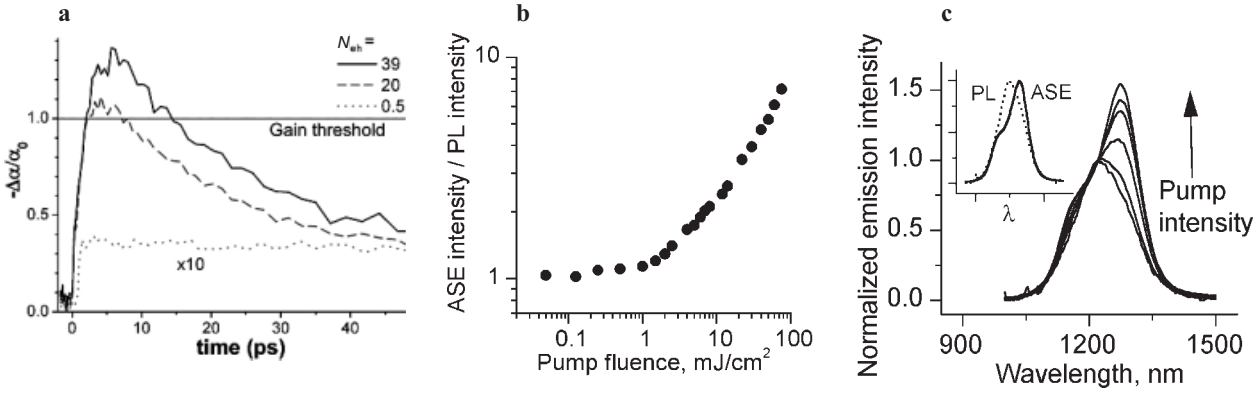

Figure 5. a) Bleaching in PbSe nanocrystals in hexane. Decay, measured at 1570 nm, increases with the pumping level; the gain lifetime near threshold is approximately 10 ps. Reproduced with permission from [30]. Copyright 2003 American Chemical Society. b) Growth, in PbS nanocrystal-based films, of amplified spontaneous emission in comparison with growth of spontaneous photoluminescence intensity with a threshold of ~1 mJ cm^{-2}. c) Evolution of the emission spectra as a function of pump intensity normalized at the point of the photoluminescence peak position for 150 μm excitation wavelength. Inset: Normalized emission spectra for low (PL) and high (ASE) pump intensities. (b,c) reproduced from [31]. Copyright 2005 Optical Society of America.

tum-dot internal efficiencies: ligand, polymer, and device fabrication strategies which preserve in the solid state the high quantum yields that are already available in solution will significantly aid this cause.

Photodetector quantum efficiencies and photovoltaic power efficiencies will benefit from a stronger internal impetus towards rapid charge separation prior to recombination. Shorter ligands, conducting ligands, and the removal of insulating ligands in favor of direct polymer–nanocrystal contacts will aid in this process, as will the use of smaller ionization-potential polymers. External quantum efficiencies will be enhanced by increasing the effective optical density at the exciton peak through increased nanocrystal loadings and increased interaction lengths via a combination of thicker nanotextured active layers and the use of resonant cavity structures.

Electro-optic modulation—either in the form of electro-absorption or electric-field-induced refractive index changes—will require the combination of a significant depth of modulation with bandwidths in the kilohertz range (friend/foe identification) and well beyond for communications applications.

Communications-wavelength lasing on a silicon substrate using gain provided by processible materials is impatiently awaited. First demonstrations will rely on a substantial optical gain per unit length, combined with sufficiently high-quality-factor cavities to enable a predominance of stimulated emission within the timeframe on which gain is available—either through the gain lifetime itself, or through a temporally stretched excitation pulse.

Biological applications of infrared quantum dots are enabled by already-demonstrated efficient, biocompatible, stable fluorophores emitting in the second tissue window. These await full exploitation in this promising application area.

Received: September 21, 2004
Final version: November 2, 2004

[1] "Electronic & Photonic Integrated Circuit (EPIC)", Announcement BAA04-15, Defense Advanced Research Projects Agency, Arlington, VA **2004**.
[2] K. Rosenbach, J. Schiller, in *IEEE 2000 Radar Conf.*, IEEE, Piscataway, NJ **2000**, p. 305.
[3] X. Gao, Y. Cui, R. M. Levenson, L. W. K. Chung, S. Nie, *Nat. Biotechnol.* **2004**, *22*, 969.
[4] Y. T. Lim, S. Kim, A. Nakayama, N. E. Stott, M. G. Bawendi, J. V. Frangioni, *Mol. Imaging* **2003**, *2*, 50.
[5] S. Kim, Y. T. Lim, E. G. Soltesz, A. M. De Grand, J. Lee, A. Nakayama, J. A. Parker, T. Mihaljevic, R. G. Laurence, D. M. Dor, L. H. Cohn, M. G. Bawendi, J. V. Frangioni, *Nat. Biotechnol.* **2004**, *22*, 93.
[6] G. O. Schlengel, F. W. Burkholder, S. A. Kleim, W. A. Beckman, B. D. Woods, J. D. Muhs, *Sol. Energy* **2004**, *76*, 359.
[7] L. M. Fraas, J. E. Avery, H. X. Huang, R. U. Martinelli, *Semicond. Sci. Technol.* **2003**, *18*, S165.
[8] M. A. Hines, G. D. Scholes, *Adv. Mater.* **2003**, *15*, 1844.
[9] F. W. Wise, *Acc. Chem. Res.* **2000**, *33*, 773.
[10] L. Bakueva, I. Gorelikov, S. Musikhin, X. S. Zhao, E. H. Sargent, E. Kumacheva, *Adv. Mater.* **2004**, *16*, 926.
[11] L. Levina, V. Sukhovatkin, S. Musikhin, S. Cauchi, E. H. Sargent, unpublished.
[12] D. Steiner, D. Katz, O. Millo, A. Aharoni, S. H. Kan, T. Mokari, U. Banin, *Nano Lett.* **2004**, *4*, 1073.
[13] D. Krapf, S.-H. Kan, U. Banin, O. Millo, A. Sa'ar, *Phys. Rev. B: Condens. Matter Mater. Phys.* **2004**, *69*, 733 011.
[14] E. Nahum, Y. Ebenstein, A. Aharoni, T. Mokari, U. Banin, N. Shimoni, O. Millo, *Nano Lett.* **2004**, *4*, 103.
[15] V. I. Klimov, A. A. Mikhailovsky, D. W. McBranch, C. A. Leatherdale, M. G. Bawendi, *Science* **2000**, *287*, 1011.
[16] M. Nirmal, B. O. Dabbousi, M. G. Bawendi, J. J. Macklin, J. K. Trautman, T. D. Harris, L. E. Brus, *Nature* **1996**, *383*, 802.
[17] C. R. Kagan, C. B. Murray, M. G. Bawendi, *Phys. Rev. B: Condens. Matter Mater. Phys.* **1996**, *54*, 8633.
[18] S. A. Crooker, J. A. Hollingsworth, S. Tretia, V. I. Klimov, *Phys. Rev. Lett.* **2002**, *89*, 18 602/1.
[19] N. Tessler, V. Medvedev, M. Kazes, S. Kan, U. Banin, *Science* **2002**, *295*, 1506.
[20] L. Bakueva, S. Musikhin, M. A. Hines, T.-W. F. Chang, M. Tzolov, G. D. Scholes, E. H. Sargent, *Appl. Phys. Lett.* **2003**, *82*, 2895.
[21] L. Bakueva, G. Konstantatos, L. Levina, S. Musikhin, E. H. Sargent, *Appl. Phys. Lett.* **2004**, *84*, 3459.
[22] J. S. Steckel, S. Coe-Sullivan, V. Bulovic, M. G. Bawendi, *Adv. Mater.* **2003**, *15*, 1862.
[23] T.-W. F. Chang, S. Musikhin, L. Bakueva, L. Levina, M. A. Hines, P. W. Cyr, E. H. Sargent, *Appl. Phys. Lett.* **2004**, *84*, 4295.
[24] T.-W. F. Chang, A. Maria, P. W. Cyr, V. Sukhovatkin, L. Levina, E. H. Sargent, *Synth. Met.*, Published Online November 21, 2004, DOI: 10.1016/j.synthmet.2004.10.003.
[25] A. Shik, G. Konstantatos, E. H. Sargent, H. E. Ruda, *J. Appl. Phys.* **2003**, *94*, 4066.
[26] A. Shik, S. Yu, E. Johnson, H. Ruda, E. H. Sargent, *Solid-State Electron.* **2002**, *46*, 61.
[27] S. A. McDonald, P. W. Cyr, L. Levina, E. H. Sargent, *Appl. Phys. Lett.* **2004**, *85*, 2089.
[28] S. A. McDonald, G. Konstantatos, S. Zhang, P. W. Cyr, E. J. D. Klem, L. Levina, E. H. Sargent, *Nat. Mater.,* Published Online January 9, 2005, DOI: 10.1038/nmat1299.
[29] B. L. Wehrenberg, P. Guyot-Sionnest, *J. Am. Chem. Soc.* **2003**, *125*, 7806.
[30] R. D. Schaller, M. A. Petruska, V. I. Klimov, *J. Phys. Chem. B* **2003**, *107*, 13 765.
[31] V. Sukhovatkin, S. Musikhin, I. Gorelikov, S. Cauchi, L. Bakueva, E. Kumacheva, E. H. Sargent, *Opt. Lett*. **2005**, *30*, 171.
[32] M. Achermann, M. A. Petruska, S. Kos, D. L. Smith, D. D. Koleske, V. I. Klimov, *Nature* **2004**, *429*, 642.
[33] L. Pavesi, L. Dal Negro, C. Mazzoleni, G. Franzo, F. Priolo, *Nature* **2000**, *408*, 400.

